THE JOURNAL OF PHYSICAL CHEMISTRY A

Article

pubs.acs.org/JPCA

Photoelectron Angular Distributions of Pyridinide: A Benchmark Application of the Mixed s−p Model to a Truly Polyatomic Anion

Lori Marie Culberson, Christopher Charles Blackstone, and Andrei Sanov*

Department of Chemistry and Biochemistry, University of Arizona, Tucson, Arizona 85721, United States

ABSTRACT: We report a photoelectron imaging study of the pyridinide anion, $C_5H_4N^-$, obtained by deprotonation of pyridine at the C4 position. The photoelectron angular distributions are used to test the theoretical formalism for photodetachment from mixed-character s−p states, demonstrating its first application to a truly polyatomic system. The mixed s−p model describes the initial state of the anion in terms of a superposition of one s orbital and one p orbital centered on the deprotonated carbon. Using the model parameter values determined from *ab initio* calculations, without any fits to the experimental data, the theory yields good quantitative agreement to the experiment. The agreement is demonstrated using either the canonical Hartree−Fock highest-occupied molecular orbital of the anion or the corresponding Dyson orbital. The results confirm the predictive power of the mixed s−p model and suggest that despite its approximate nature it captures the essential physics of the photoemission process.

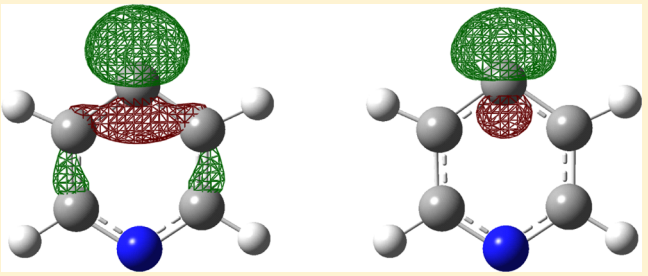

1. INTRODUCTION

Representation of molecular orbitals (MO) in terms of superpositions of atomic functions is a common approach to describing the electronic structure of molecules. It may involve the orbitals of individual atoms or the atomic-like functions centered anywhere in the molecular frame. Both variants are based on the same mathematical concept of basis-set expansion.

In a related realm, the conceptual description of chemistry often involves defining the primary character of the MOs that control the molecular bonding structures. For example, hybrid orbitals have long been used for predicting molecular geometries and reactivity. Such general approaches have indisputable theoretical and pedagogical value in introducing the fundamental concepts of chemistry. While many modern theoretical methods aim to provide an increasingly accurate and detailed description of the electronic structure (demanding ever increasing computing power and basis sets with myriads of functions), the ultimate goal of scientific exploration remains the conceptual understanding of the big picture, such as the dominant character of chemical bonds.

A variety of experimental methods aim at the electronic structure of molecules. Coupled with theoretical modeling, the experiments expand our understanding of molecular bonding motifs. Photoelectron imaging, in particular, focuses not only on photoelectron spectra[1,2] (and the energy levels that they reflect) but also on the photoelectron angular distributions (PAD),[3,4] reflecting the symmetry properties of the electronic wave functions and the physics of the photoemission process.[5]

Photodetachment from mixed-character states of negative ions, involving, for example, the sp^x hybrid orbitals, presents an interesting conceptual problem. In the limiting cases of atomic or atomic-like states (with defined or effective values of the orbital angular momentum quantum number l), the PADs can be described using the Cooper−Zare model,[6,7] which is based on the central-potential theory of Bethe.[8,9] While a direct application of the Cooper−Zare formula[6,7] requires the evaluation of transition matrix elements (not a trivial undertaking in its own right),[10] a more practical approach was proposed by Hanstorp et al.,[11] who assumed that the relative scaling of the partial-wave cross sections follows the Wigner law.[12] Within this formalism, photodetachment from an s or s-like orbital is generally expected to yield a parallel angular distribution, described by a positive value of the photoelectron anisotropy parameter β, with a limiting value of 2 for a pure s orbital.[6,7,13] Photodetachment from a p or p-like orbital, on the other hand, is generally expected to yield a perpendicular PAD (in the moderate electron kinetic energy, eKE, regime),[11,14,15] with the value of $\beta < 0$ varying with eKE due to the interference of s and d partial waves.[6,7]

Until recently, no practical analogue of the Cooper−Zare formula[6,7] similar to Hanstorp's equation[11] had existed for the photodetachment from molecular orbitals described by superpositions of more than one initial l value.[16] To this end, our group has developed an approximate formalism for photodetachment from mixed-character s−p states. Initially proposed by Grumbling et al.[17] for the case of solvation-induced polarization of the initial state, it was shown to be applicable to PADs resulting from a broad class of hybrid sp^x molecular orbitals.[18] The formalism is rooted in a central-atom approximation, which considers the s and p functions localized

Special Issue: Curt Wittig Festschrift

Received: March 12, 2013
Revised: April 18, 2013
Published: April 23, 2013

on a single center in the parent molecular anion. This assumption works well for certain MOs, such as the HOMO−1 of NH_2^- (localized predominantly on the "central" nitrogen atom), but is less applicable to other similar-size anion orbitals, such as the HOMO−1 of CCl_2^- (which includes non-negligible contributions of Cl orbitals, leading to the breakdown of the central-atom approximation).[18]

In this paper, we apply the mixed s−p model[17,18] to a more complex system, the pyridinide anion, $C_5H_4N^-$. This closed-shell species is derived from deprotonation of pyridine, C_5H_5N, at the C4 position.[19,20] The optimized molecular geometry and the a_1 symmetry HOMO of $C_5H_4N^-$, calculated[21] at the CCSD/6-31+G* level of theory, are illustrated in Figure 1a. As

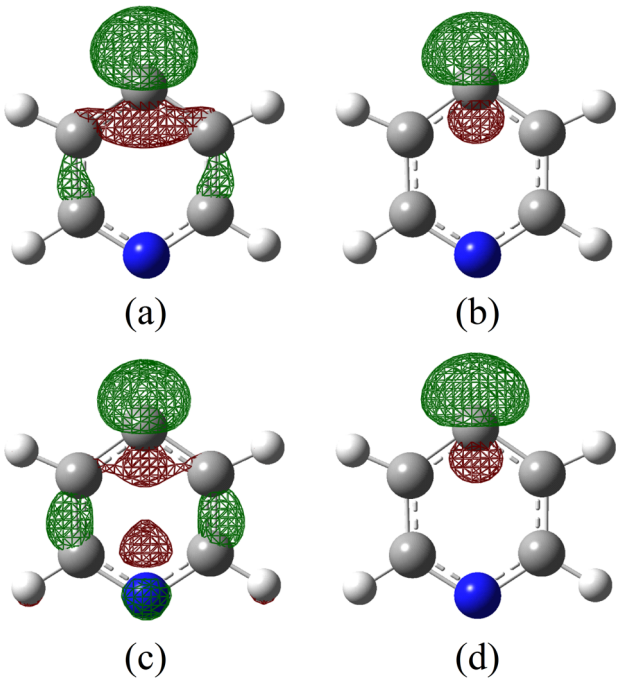

Figure 1. (a) The ground-state geometry of the pyridinide anion, optimized at the CCSD/6-31+G* level of theory, superimposed with an isosurface plot of the HOMO. The dominant character of the orbital is a hybrid s−p function localized on the C4 center (the deprotonated C atom opposing the Nitrogen center). (b) The model wave function obtained as a least-squares fit of ψ_{sp} defined in the text to the *ab initio* orbital shown in panel a. The fit yields an effective nuclear charge ξ = 3.10 and a fractional p character value f = 0.88. (c) The Dyson orbital corresponding to the X $^1A_1 \rightarrow$ X $^2A_1$ photodetachment transition, computed at the EOM-IP-CCSD/6-31+G* level of theory. (d) The corresponding model wave function ψ_{sp} with ξ = 3.13 and f = 0.86, obtained by fitting a superposition of hydrogenic 2s and 2p functions on the C4 center to the Dyson orbital shown in panel c. The isosurface value for all orbitals shown in panels a−d is 0.08.

expected, the dominant contribution to the HOMO is due to the in-plane sp^x hybridized orbital of the deprotonated carbon center (C4). Electron emission from this initial orbital is a good candidate for modeling using the s−p mixing approach.

Wren et al. reported the vibrationally resolved photoelectron spectra of pyridinide.[20] From their measurements, Franck−Condon calculations, and thermochemical analysis, they determined the adiabatic electron affinity of the pyridinyl radical, EA($^\bullet C_5H_4N$) = 1.480 ± 0.006 eV, and the C−H bond dissociation energy of pyridine, 110.4 ± 2.0 kcal/mol.

In the present work, we approach this system from an entirely different angle. By measuring and modeling the photoelectron angular distributions, we probe the properties of the pyridinide anion HOMO and demonstrate the first application of the s−p mixing formalism to a truly polyatomic system. A very good (nearly perfect) quantitative agreement between the experiment and the model is achieved using the *ab initio* properties of the system without any adjustable parameters. Such agreement confirms the predictive power of the mixed s−p model and suggests that despite its approximate nature it does capture the essential physics of the photoemission process.

2. EXPERIMENTAL AND THEORETICAL METHODS

The experiments were carried out using the negative ion photoelectron imaging spectrometer described in detail previously.[22,23] The ions were generated by introducing a neutral precursor gas mixture into the high-vacuum ion source chamber through a pulsed supersonic nozzle (General Valve, series 9) operated at a repetition rate of 20−70 Hz and a 20 psi backing pressure. In the present experiments, the precursor gas mixture consisted of room-temperature pyridine vapor seeded in argon carrier gas, with minor O_2 and water contaminants from ambient air in the gas delivery lines. Negative ions were formed via slow secondary electron attachment following bombardment of the neutral precursors with high-energy (1 keV) electrons. Atomic oxygen anions generated from O_2 impurities assisted with the deprotonation of pyridine. The anions were separated and characterized in the time-of-flight mass spectrometer.

Anion photodetachment was performed at 306, 355, 392, 532, 612, and 777 nm. The 777 nm radiation was the fundamental output of an amplified Ti:sapphire laser (Spectra Physics; <1 mJ/pulse, 100 fs pulse width). The 392 nm light was obtained by frequency doubling the fundamental output of the same laser. The 532 and 355 nm radiation was the second and third harmonics, respectively, of a Nd:YAG laser (Spectra Physics; 25 and 5 mJ/pulse, respectively, ∼6 ns pulse duration). The 612 nm radiation was the fundamental output of a Continuum, Inc., Surelight II-20 Nd:YAG pumped (532 nm) ND6000 dye laser, operating on the Rhodamine 640 dye and delivering 20 mJ, ∼10 ns duration pulses. The 306 nm light was obtained by frequency doubling the above output of the dye laser. The laser beams were mildly focused using a 2 m focal length lens positioned approximately 1.2 m before the laser−ion interaction region.

Details of the photoelectron[2] imaging[24,25] assembly are described elsewhere.[22,23] Most photoelectron images in this work were recorded with the repeller, middle, and acceleration electrodes of the velocity-map[26] imaging lens at −330, 0, and 900 V, respectively. Additionally, some 532 nm images were taken with the −110/0/300 V potentials for improved resolution. The images reported in the next section each correspond to multiple experimental runs combined to span ∼10^6 experimental cycles at each wavelength. The results were analyzed by means of the inverse Abel transformation[25] using the BASEX software package.[27]

Details of the mixed s−p model were published previously.[17,18] For geometry optimization and calculation of the canonical Hartree−Fock HOMO of $C_5H_4N^-$, the Gaussian 09 software package[21] was used. The corresponding Dyson orbital was computed using the EOM-IP-CCSD method[28] implemented in Q-Chem.[29]

dx.doi.org/10.1021/jp402507v | J. Phys. Chem. A 2013, 117, 11760−11765

3. RESULTS

Photoelectron imaging experiments on the pyridinide anion were carried out at 306, 355, 392, 532, 612, and 777 nm. The representative photoelectron images (corresponding to 355, 532, and 777 nm) are shown in Figure 2 alongside the Abel-

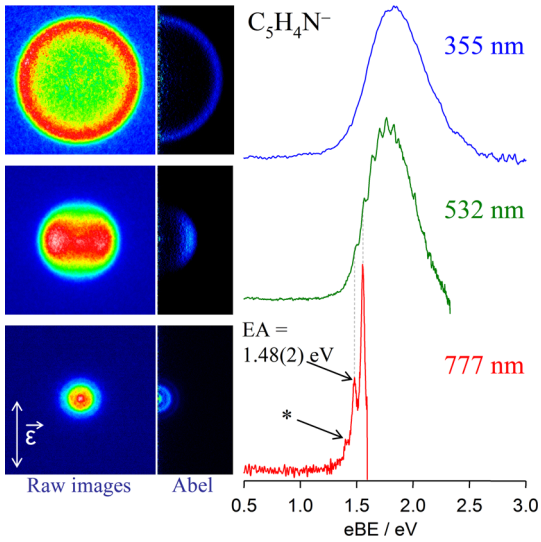

Figure 2. Raw (left) and Abel-inverted (middle) photoelectron images and spectra (right) for photodetachment of pyridinide obtained at 355, 532, and 777 nm. The polarization axis is vertical in the plane of the images, as indicated by the double arrow in the bottom left corner. Only the right halves of the Abel-inverted images are shown. The peak marked EA in the 777 nm spectrum corresponds to the adiabatic electron affinity of $^{\bullet}C_5H_4N$, EA = 1.48 ± 0.02 eV. The peak marked with an * is a vibrational hot band.

reconstructed data and photoelectron energy spectra. Only the right halves of the reconstructed images are shown, as the results are intrinsically symmetric with respect to the central axis defined by the laser polarization direction. The photoelectron spectra are plotted versus electron binding energy, eBE = $h\nu$ − eKE. All transitions observed at each wavelength studied correspond to removing an electron from the a_1 HOMO of the anion to form the ground state of the pyridinyl σ-radical.

Partial vibrational resolution in the 777 nm data allows for determination of the adiabatic electron affinity of the radical, EA($^{\bullet}C_5H_4N$) = 1.48 ± 0.02 eV. This value agrees with the previous report by Wren et al., EA = 1.480 ± 0.006 eV.[20] There is a lower-eBE peak seen in both our data (marked with an asterisk in Figure 2), and the results of Wren et al. Franck–Condon analysis unambiguously showed that this peak (*) is a hot band due to vibrationally excited anions.[20] The observed progression corresponds to the excitation of the ν_9 in-plane ring-distorting vibrational mode of the neutral radical, with an average spacing of 0.075 ± 0.003 eV (605 ± 25 cm^{-1}). This agrees with the value of ν_9 = 600 ± 20 cm^{-1} reported by Wren et al.[20]

In contrast to Wren et al.'s report,[20] the main focus of this work is the energy-dependent photoelectron angular distributions. Our interpretation of the PADs is based on the assumption that, for a given electronic transition, the photoelectron anisotropy is a signature of the parent orbital. We will neglect vibronic coupling, since its effects are mostly averaged out in the observed congested transitions. Under this assumption, the anisotropy parameter β does not depend explicitly on the vibrational state of the resulting neutral molecule. It does, however, depend on it implicitly, through the corresponding variation of photoelectron kinetic energy. Under these assumptions, β (as a signature of the parent orbital) is viewed as an explicit function of eKE rather than eBE, i.e., $\beta = \beta(\varepsilon)$, where $\varepsilon \equiv$ eKE. By analyzing the photodetachment at various wavelengths, we examine this dependence over a wide energy range.

To determine the eKE-dependent β values, the PADs observed at 777, 612, and 532 nm were analyzed in narrow (0.06 eV) spectral intervals chosen to coincide approximately with the partially resolved vibrational peaks. The 392, 355, and 306 nm PADs were integrated over the full width at half-maximum of the entire photodetachment band, and the resulting β values were assigned to eKEs of the corresponding band maxima. Thus determined $\beta(\varepsilon)$ values are plotted in Figure 3, with the different-color symbols representing data obtained at different wavelengths.

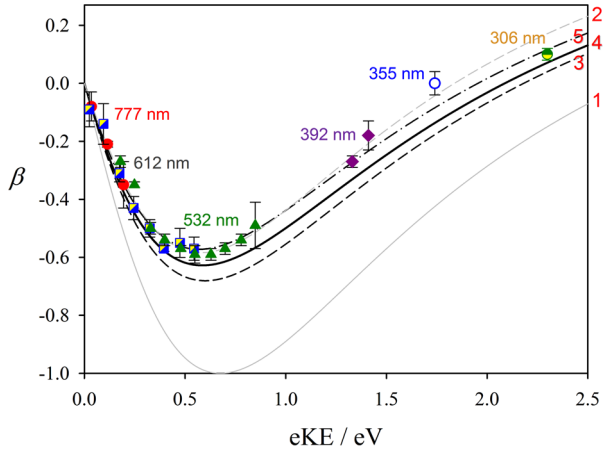

Figure 3. Symbols: experimental photoelectron anisotropy parameter values resulting from pyridinide photodetachment plotted versus electron kinetic energy. Red circles: 777 nm. Yellow/blue squares: 612 nm. Green triangles: 532 nm. Purple diamonds: 392 nm. Blue open circle: 355 nm. Green/yellow circles: 306 nm. Model curves are marked with red numerals 1–5 along the right border of the graph. Curves 1 and 2 are derived from the central potential model (eq 1) with l = 1 and A = 0.75 eV^{-1}. Curve 1 (solid gray) assumes $\cos(\delta_2 - \delta_0) = 1$, while for curve 2 (gray dash) $\cos(\delta_2 - \delta_0) = 0.68$. Curves 3–5 are mixed s–p model predictions (eqs 2 and 3), assuming A = 0.75 eV^{-1} and B/A = 8/3. Curve 3 (black dash): f = 0.88 (corresponding to the model ψ_{sp} function shown in Figure 1b) and $\cos(\delta_2 - \delta_0) = 1$. Curve 4 (black solid): f = 0.86 (corresponding to the model ψ_{sp} function shown in Figure 1d) and $\cos(\delta_2 - \delta_0) = 1$. Curve 5 (black dash–dot): f = 0.86 and $\cos(\delta_2 - \delta_0) = 0.95$.

4. DISCUSSION

We analyze the observed PADs within two different conceptual frameworks. First, in section 4.1 the parent molecular orbital is represented as a p-like function within the Copper and Zare central-potential model.[6,11] Since the $C_5H_4N^-$ HOMO (Figure 1a) is hardly a simple atomic orbital with a defined l quantum number, this approach is obviously deficient. Therefore, a more appropriate, yet still conceptually straightforward description treating the initial MO as an s and p hybrid orbital is presented in section 4.2.

dx.doi.org/10.1021/jp402507v | J. Phys. Chem. A 2013, 117, 11760–11765

4.1. Central-Potential Model. In Hanstorp et al.'s formulation[11] of the Cooper–Zare central-potential model,[6] the photodetachment anisotropy parameter can be modeled as an explicit function of electron kinetic energy:

$$\beta(\varepsilon) = \frac{l(l-1) + (l+1)(l+2)A^2\varepsilon^2 - 6l(l+1)A\varepsilon\cos(\delta_{l+1} - \delta_{l-1})}{(2l+1)[l + (l+1)A^2\varepsilon^2]} \quad (1)$$

where l is the orbital angular momentum of the initial (bound) state, A is a proportionality constant reflecting the relative scaling of the outgoing $l + 1$ and $l - 1$ partial waves, and $\delta_{l+1} - \delta_{l-1}$ is the corresponding phase shift.

The Cooper–Zare central potential model does not apply, in general, to molecular systems. Nonetheless, eq 1 has been used successfully to model the anisotropy of molecular-anion photodetachment in cases where the initial state can be assigned an effective l value (e.g., $l = 2$ for the 2p π_g* HOMO of O_2^-).[10,30−32] However, the range of molecular systems for which this approach is useful[33] is rather limited.

The a_1 symmetry HOMO of $C_5H_4N^-$ shown in Figure 1a has a dominant contribution from a 2p orbital of the deprotonated carbon atom. Therefore, two of the model curves in Figure 3, curves 1 and 2, were calculated using the Cooper–Zare model, eq 1, with $l = 1$. The A coefficient value of $A = 0.75$ eV^{-1}, corresponding to $C^-(^4S)$ photodetachment, was used for both curves, accounting for the similar electron binding energies in $C^-(^4S)$ and $C_5H_4N^-$.[18] Curve 1 further neglects any phase-shift between the s and d partial waves, i.e., $\cos(\delta_2 - \delta_0) = 1$. This calculation captures the approximate location of the minimum observed in the experimental $\beta(\varepsilon)$ dependence, but the agreement with the experimental results is poor.

While the energy position of the minimum of a curve defined by eq 1 is controlled by A, the depth of the minimum is affected by the cosine of the phase shift. Curve 2 in Figure 3 was calculated using eq 1 with the same l and A values as those used for curve 1, but using the s–d phase-shift as an adjustable parameter. The corresponding fit to the measured $\beta(\varepsilon)$ values yields a good agreement with the experimental data, but requires a very large phase-shift, $\cos(\delta_2 - \delta_0) = 0.65$. For comparison, in the previous applications of the Cooper–Zare model to molecular anions with effective l values, the accepted phase-shift was typically significantly smaller, usually corresponding to $\cos(\delta_2 - \delta_0) \sim 0.95$.

4.2. Mixed s–p Model. We now provide a quantitative interpretation of the experimental results using the recently proposed generalization of the Cooper–Zare equation to s–p mixed-character states.[17,18] It is clear by inspection of Figure 1a that a superposition of s and p functions is a more valid description of the pyridinide anion HOMO than the singular $l = 1$ approximation employed in section 4.1. In fact, the HOMO of $C_5H_4N^-$ can be nominally described as a predominantly sp^2 hybrid orbital centered on the deprotonated carbon, although the actual amount of the s character warrants a more in-depth examination. The addition of partial s character to the model description of the initial anion orbital opens the p detachment channel, not accounted for by the Cooper–Zare formalism used in section 4.1. Here we show that a quantitative agreement between the mixed s–p model prediction and the experimental data can be achieved without resorting to any additional assumptions or large phase-shifts.

The mixed s–p model of photodetachment from a hybrid orbital predicts the following dependence of the anisotropy parameter (β) on eKE (ε):[17,18]

$$\beta = \frac{2Z\varepsilon + 2A\varepsilon^2 - 4\varepsilon\cos(\delta_2 - \delta_0)}{A^{-1} + 2A\varepsilon^2 + Z\varepsilon} \quad (2)$$

where A has the same meaning as in eq 1 for the $l = 1$ case, i.e., it describes the relative scaling of the p → d and p → s photodetachment channels with energy, while Z is a new parameter introduced in our recent work:[18]

$$Z = \frac{1-f}{f}\frac{B}{A} \quad (3)$$

In eq 3, f is the p fraction, i.e., the fractional p character of the initial MO, while B is a constant, similar to A, describing the relative scaling of the s → p and p → s photodetachment channels.[17] Hence, Z describes the relative intensities of the s → p and p → s, d channels (via B/A), weighted by the contributions of the s and p components to the initial state, $(1 - f)/f$. Note further that eq 2 transforms into eq 1 for $l = 1$ in the limit of $Z = 0$, corresponding to a pure p state limit. It also simplifies to eq 1 for $l = 0$ (i.e., $\beta = 2$) in the asymptotic limit of $Z \to \infty$, which corresponds to a pure s state.[18] Thus, both the s and p limits of the mixed s–p model are consistent with the Cooper–Zare central-potential formula.

As shown previously, the B/A ratio for the calculation of Z depends on the types of the s and p components of the parent hybrid orbital. It is particularly sensitive to the long-range behavior of the anionic wave function.[18] However, under certain assumptions, the B/A ratio for a 2s–2p mixed-character orbital has been shown to simplify to $B/A = 8/3$.[18] This value will be used in the following analysis.

To determine the fractional p character of the parent orbital, f in eq 3, we construct a model orbital ψ_{sp}, defined as a superposition of hydrogenic 2s and 2p functions (one of each) on the deprotonated carbon center (C4) in $C_5H_4N^-$. The spatial extent of the hydrogenic functions is described by an effective nuclear charge ξ, assumed to be the same for both the 2s and 2p contributions (to be consistent with the above $B/A = 8/3$ value).[18] Given a fractional p character f, the amplitudes of the 2s and 2p contributions to ψ_{sp} are $(1 - f)^{1/2}$ and f, respectively.[17,18] The model orbital is thus defined by two variable parameters, ξ and f, which were used to optimize the overlap of ψ_{sp} with the HOMO of $C_5H_4N^-$.

The least-squares fit of ψ_{sp} to the CCSD/6-31+G* HOMO shown in Figure 1a yielded the optimal values of $\xi = 3.10$ and $f = 0.88$. The effective charge of 3.10 compares favorably to the Slater's rules[34] predictions of 3.25 and 2.9 for the $n = 2$ electrons in C and C^-, respectively. As the excess charge in the pyridinide anion is partially delocalized, the ξ value is indeed expected to be intermediate between those for the atomic neutral and singly charged anion. Similar fits to the HOMO calculated at the MP2/aug-cc-pVDZ and B3LYP/aug-cc-pVDZ levels yielded $\xi = 3.10$, $f = 0.88$ and $\xi = 3.13$, $f = 0.85$, respectively. All fit results are summarized in Table 1.

An isosurface plot of the model orbital fit to the CCSD/6-31+G* HOMO of pyridinide, i.e., $\psi_{sp}(\xi = 3.10, f = 0.88)$, is plotted in Figure 1b, alongside the HOMO itself. As expected, the model orbital correctly captures the hybrid character of the dominant part of the HOMO centered on C4, while missing the delocalized parts of the orbital.

dx.doi.org/10.1021/jp402507v | J. Phys. Chem. A 2013, 117, 11760−11765

Table 1. Optimized Fractional p Character (f) and Effective Nuclear Charge (ξ) Describing the Model Function ψ_{sp} Defined in the Text[a]

method/basis set	f	ξ
CCSD/6-31+G*[b]	0.88	3.10
EOM-IP-CCSD/6-31+G* (Dyson)[b]	0.86	3.13
MP2/aug-cc-pVDZ[b]	0.88	3.10
B3LYP/aug-cc-pVDZ[c]	0.85	3.13

[a]The parameter values are determined via least-squares fitting of $\psi_{sp}(f, \xi)$ to the pyridinide anion HOMO or the corresponding Dyson orbital, computed at the indicated levels of theory. The confidence limits are ±0.01 for f and ±0.02 for ξ. [b]Calculations are carried out using the C_{2v} symmetry geometry of the pyridinide anion optimized at the MP2/aug-cc-pVDZ level. [c]Calculations are carried out using the C_{2v} symmetry geometry of the pyridinide anion optimized at the B3LYP/aug-cc-pVDZ level.

Note that the above fractional p character value f does not accurately reflect the hybridization state of the C4 atom in pyridinide. The f value is determined by fitting the model orbital to the *ab initio* HOMO, including the contributions of the neighboring carbon atoms to the MO in the vicinity of C4. Calculating f from the molecular-orbital coefficients for the s- and p-type functions of C4 only, contributing to the HOMO, yields a significantly smaller f value of ∼0.6. The constructive contributions of the neighboring-atom (C3 and C5) orbitals to the HOMO density just below the C4 center (in the Figure 1 orientation) have the effect of partially symmetrizing the orbital with respect to C4, thus increasing the effective p character of the model orbital without affecting the intrinsic hybridization state of C4. It can be said that the f = 0.85−0.88 values summarized in Table 1 include corrections for the partial breakdown of the central-atom approximation implicit in the model.[18]

Substituting f = 0.88 (CCSD/6-31+G* or MP2/aug-cc-pVDZ in Table 1) and B/A = 8/3 into eq 3 yields Z = 0.36. This Z value, together with A = 0.75 eV^{-1} and assuming no phase shift, allows modeling the eKE dependence of the anisotropy parameter β using eq 2. The resulting $\beta(\varepsilon)$ prediction is plotted in Figure 3 as curve 3. It is in nearly quantitative agreement with the experimental results. Remarkably, using f = 0.85 (B3LYP/aug-cc-pVDZ in Table 1) instead of f = 0.88 yields an essentially perfect agreement between the model and the experiment. Although the corresponding curve is not shown in Figure 3, it is very similar to curve 5 shown there.

Further improvement of the model can be achieved by taking into account the electron correlation and relaxation effects inherent in the photodetachment of the many-electron system. To this end, without much additional effort the canonical Hartree−Fock HOMO used in the above analysis can be replaced with the corresponding Dyson orbital.[35−37] The Dyson orbital for the lowest-energy photodetachment transition in $C_5H_4N^-$ was computed using the EOM-IP-CCSD/6-31+G* method[28] implemented in the Q-Chem software package.[29] The result is shown in Figure 1c. Despite some differences between the Dyson orbital and the corresponding Hartree−Fock orbital in Figure 1a, the resulting model parameters are not too different (Table 1). The model function representing the Dyson orbital, $\psi_{sp}(f = 0.86; \xi = 3.13)$, is plotted in Figure 1d, while the mixed s−p model prediction using the Dyson orbital f value (with no phase shift) is shown in Figure 3 as curve 4.

An important point of this discussion is that curves 3 and 4 in Figure 3 represent unaltered model *predictions*, calculated from first principles without any adjustable parameters or fitting to experimental data (unlike the Cooper−Zare model fit given by curve 2). The only fit involved in the calculation of curves 3 and 4 is the determination of the p character values by fitting the model orbital ψ_{sp} to the calculated Hartree−Fock or Dyson orbitals. This procedure, reducing the orbitals to a superposition of the 2s and 2p functions on C4, is purely *ab initio* in nature, independent of the experimental results obtained in this work; it is not a model fit to the data. Comparing curves 3 and 4 to the experimental data in Figure 3 indicates a nearly quantitative agreement, particularly in the Dyson orbital case (curve 4), achieved without any adjustable parameters. The agreement is very satisfying indeed, suggesting that the mixed s−p model correctly captures the physics of the photodetachment process from the hybrid initial state.

Finally, one may question the assumption of a zero phase-shift used in the calculation of curves 3 and 4. Although the calculation of the correct phase-shift magnitude is beyond the scope of this work, in many previous attempts to model anion photodetachment using the Cooper−Zare formula, the phase-shift corresponds to $\cos(\delta_2 - \delta_0)$ in the 0.86−0.96 range.[10,11,14,30−32] Curve 5 in Figure 3 was calculated using eq 2 with the Dyson orbital parameters (f = 0.86) and cosine of the phase shift set arbitrarily to 0.95. Again, the resulting agreement with the experiment is quite remarkable, but we caution that, in contrast to curves 3 and 4, curve 5 does include an adjustable parameter (the above cosine), with no solid justification given for the value used.

5. CONCLUSIONS

The photoelectron angular distributions obtained in this photoelectron imaging study of the pyridinide anion have been used as a benchmark for testing the theoretical formalism of photodetachment from mixed-character s−p states.[17,18] By measuring and modeling the PADs, we probe the hybridization of the pyridinide anion HOMO and demonstrate the first application of the s−p mixing formalism to a truly polyatomic system.

The observed PADs have been analyzed within two conceptual frameworks. First, viewing the parent MO as a predominantly p-like function within the Hanstorp et al. formulation[11] of the Copper−Zare central-potential model[6−8] with effective l = 1 yields poor agreement with the experiment, unless a substantial phase-shift between the s and d photodetachment partial waves is assumed, corresponding to $\cos(\delta_2 - \delta_0) = 0.65$ in eq 1. This disagreement is not surprising, since the $C_5H_4N^-$ HOMO (Figure 1a) is hardly a simple p orbital.

Using the mixed s−p model,[17,18] which describes the parent MO as a superposition of one s orbital and one p orbital centered on the deprotonated carbon, yields a nearly perfect quantitative agreement between the theory and the experiment. Only the *ab initio* properties of the system are used in the modeling, with no adjustable parameters. We demonstrate good agreement between the model and the experiment by viewing the photodetachment as a one-electron process involving the Hartree−Fock HOMO of the anion, and an even better (albeit only marginally better) agreement using the corresponding Dyson orbital.

dx.doi.org/10.1021/jp402507v | J. Phys. Chem. A 2013, 117, 11760−11765

The results confirm the predictive power of the mixed s−p model and suggest that despite its approximate nature it captures the essential physics of the photoemission process.

AUTHOR INFORMATION

Corresponding Author

*E-mail: sanov@u.arizona.edu.

Notes

The authors declare no competing financial interest.

ACKNOWLEDGMENTS

This work was supported by the U.S. National Science Foundation (Grant CHE-1011895). L.M.C. acknowledges the support of the State of Arizona TRIF program via the Imaging and Photonics Fellowships. We express special thanks to the leaders and employees of Q-Chem, Inc., for providing an evaluation copy of the software, and to the anonymous reviewer of our previous paper[18] for suggesting that Dyson orbitals be included in our work.

REFERENCES

(1) Eland, J. H. D. *Photoelectron Spectroscopy: An Introduction to Ultraviolet Photoelectron Spectroscopy in the Gas Phase*; Butterworths: London, 1984.

(2) Ervin, K. M.; Lineberger, W. C. Photoelectron Spectroscopy of Negative Ions. In *Advances in Gas Phase Ion Chemistry*; Adams, N. G., Babcock, L. M., Eds.; JAI Press: Greenwich, 1992; Vol. *1*, pp 121.

(3) Cooper, J.; Zare, R. N. Photoelectron Angular Distributions. In *Atomic Collision Processes*; Geltman, S., Mahanthappa, K. T., Brittin, W. E., Eds.; Gordon and Breach, Science Publishers: New York, London, Paris, 1968; Vol. *XI-C*, pp 317−337.

(4) Reid, K. L. Photoelectron Angular Distributions. *Annu. Rev. Phys. Chem.* **2003**, *54*, 397−424.

(5) Sanov, A.; Mabbs, R. Photoelectron Imaging of Negative Ions. *Int. Rev. Phys. Chem.* **2008**, *27*, 53−85.

(6) Cooper, J.; Zare, R. N. Angular Distributions in Atomic Anion Photodetachment. *J. Chem. Phys.* **1968**, *48*, 942−943.

(7) Cooper, J.; Zare, R. N. Angular Distributions in Atomic Anion Photodetachment (Erratum). *J. Chem. Phys.* **1968**, *49*, 4252.

(8) Bethe, H. A. *Handb. Phys.* **1933**, *24*, 483.

(9) Bethe, H. A.; Salpeter, E. E. *Quantum Mechanics of One- and Two-Electron Atoms*; Springer-Verlag; Academic Press Inc.: Berlin; New York, 1957.

(10) Reed, K. J.; Zimmerman, A. H.; Andersen, H. C.; Brauman, J. I. Cross Sections for Photodetachment of Electrons from Negative Ions near Threshold. *J. Chem. Phys.* **1976**, *64*, 1368−1375.

(11) Hanstorp, D.; Bengtsson, C.; Larson, D. J. Angular Distributions in Photodetachment from O^-. *Phys. Rev. A* **1989**, *40*, 670−675.

(12) Wigner, E. P. On the Behavior of Cross Sections near Thresholds. *Phys. Rev.* **1948**, *73*, 1002−1009.

(13) Grumbling, E. R.; Mabbs, R.; Sanov, A. Photoelectron Imaging as a Quantum Chemistry Visualization Tool. *J. Chem. Educ.* **2011**, *88*, 1515−1520.

(14) Mabbs, R.; Surber, E.; Sanov, A. Photoelectron Anisotropy and Channel Branching Ratios in the Detachment of Solvated Iodide Cluster Anions. *J. Chem. Phys.* **2005**, *122*, 054308.

(15) Cavanagh, S. J.; Gibson, S. T.; Gale, M. N.; Dedman, C. J.; Roberts, E. H.; Lewis, B. R. High-Resolution Velocity-Map-Imaging Photoelectron Spectroscopy of the O- Photodetachment Fine-Structure Transitions. *Phys. Rev. A* **2007**, *76*, 052708.

(16) Buckingham, A. D.; Orr, B. J.; Sichel, J. M. Angular Distribution and Intensity in Molecular Photoelectron Spectroscopy. 1. General Theory for Diatomic Molecules. *Philos. Trans. R. Soc., A* **1970**, *268*, 147−157.

(17) Grumbling, E. R.; Sanov, A. Photoelectron Angular Distributions in Negative-Ion Photodetachment from Mixed s−p States. *J. Chem. Phys.* **2011**, *135*, 164302.

(18) Sanov, A.; Grumbling, E. R.; Goebbert, D. J.; Culberson, L. M. Photodetachment Anisotropy for Mixed s−p Orbitals: 8/3 and Other Fractions. *J. Chem. Phys.* **2013**, *138*, 054311.

(19) Schafman, B. S.; Wenthold, P. G. Regioselectivity of Pyridine Deprotonation in the Gas Phase. *J. Org. Chem.* **2007**, *72*, 1645−1651.

(20) Wren, S. W.; Vogelhuber, K. M.; Garver, J. M.; Kato, S.; Sheps, L.; Bierbaum, V. M.; Lineberger, W. C. C−H Bond Strengths and Acidities in Aromatic Systems: Effects of Nitrogen Incorporation in Mono-, Di-, and Triazines. *J. Am. Chem. Soc.* **2012**, *134*, 6584−6595.

(21) Frisch, M. J.; Trucks, G. W.; Schlegel, H. B.; Scuseria, G. E.; Robb, M. A.; Cheeseman, J. R.; Scalmani, G.; Barone, V.; Mennucci, B.; Petersson, G. A. et al. *Gaussian 09*, Revision A.1; Gaussian, Inc.: Wallingford, CT, 2009.

(22) Surber, E.; Sanov, A. Photoelectron Imaging Spectroscopy of Molecular and Cluster Anions: CS_2^- and $OCS^-(H_2O)_{1,2}$. *J. Chem. Phys.* **2002**, *116*, 5921−5924.

(23) Mabbs, R.; Surber, E.; Sanov, A. Photoelectron Imaging of Negative Ions: Atomic Anions to Molecular Clusters. *Analyst* **2003**, *128*, 765−772.

(24) Chandler, D. W.; Houston, P. L. Two-Dimensional Imaging of State-Selected Photodissociation Products Detected by Multiphoton Ionization. *J. Chem. Phys.* **1987**, *87*, 1445−1447.

(25) Heck, A. J. R.; Chandler, D. W. Imaging Techniques for the Study of Chemical-Reaction Dynamics. *Annu. Rev. Phys. Chem.* **1995**, *46*, 335−372.

(26) Eppink, A. T. J. B.; Parker, D. H. Velocity Map Imaging of Ions and Electrons Using Electrostatic Lenses: Application in Photoelectron and Photofragment Ion Imaging of Molecular Oxygen. *Rev. Sci. Instrum.* **1997**, *68*, 3477−3484.

(27) Dribinski, V.; Ossadtchi, A.; Mandelshtam, V. A.; Reisler, H. Reconstruction of Abel-Transformable Images: The Gaussian Basis-Set Expansion Abel Transform Method. *Rev. Sci. Instrum.* **2002**, *73*, 2634−2642.

(28) Krylov, A. I. Equation-of-Motion Coupled-Cluster Methods for Open-Shell and Electronically Excited Species: The Hitchhiker's Guide to Fock Space. *Annu. Rev. Phys. Chem.* **2008**, *59*, 433−462.

(29) Shao, Y.; Molnar, L. F.; Jung, Y.; Kussmann, J.; Ochsenfeld, C.; Brown, S. T.; Gilbert, A. T. B.; Slipchenko, L. V.; Levchenko, S. V.; O'Neill, D. P.; et al. Advances in Methods and Algorithms in a Modern Quantum Chemistry Program Package. *Phys. Chem. Chem. Phys.* **2006**, *8*, 3172−3191.

(30) Akin, F. A.; Schirra, L. K.; Sanov, A. Photoelectron Imaging Study of the Effect of Monohydration on O_2^- Photodetachment. *J. Phys. Chem. A* **2006**, *110*, 8031−8036.

(31) Mabbs, R.; Mbaiwa, F.; Wei, J.; Van Duzor, M.; Gibson, S. T.; Cavanagh, S. J.; Lewis, B. R. Observation of Vibration-Dependent Electron Anisotropy in O_2^- Photodetachment. *Phys. Rev. A* **2010**, *82*, 011401.

(32) Van Duzor, M.; Mbaiwa, F.; Wei, J.; Singh, T.; Mabbs, R.; Sanov, A.; Cavanagh, S. J.; Gibson, S. T.; Lewis, B. R.; Gascooke, J. R. Vibronic Coupling in the Superoxide Anion: The Vibrational Dependence of the Photoelectron Angular Distribution. *J. Chem. Phys.* **2010**, *133*, 174311.

(33) Surber, E.; Mabbs, R.; Sanov, A. Probing the Electronic Structure of Small Molecular Anions by Photoelectron Imaging. *J. Phys. Chem. A* **2003**, *107*, 8215−8224.

(34) Slater, J. C. Atomic Shielding Constants. *Phys. Rev.* **1930**, *36*, 0057−0064.

(35) Ortiz, J. V. Brueckner Orbitals, Dyson Orbitals, and Correlation Potentials. *Int. J. Quantum Chem.* **2004**, *100*, 1131−1135.

(36) Oana, C. M.; Krylov, A. I. Dyson Orbitals for Ionization from the Ground and Electronically. *J. Chem. Phys.* **2007**, *127*, 234106.

(37) Oana, C. M.; Krylov, A. I. Cross Sections and Photoelectron Angular Distributions in Photodetachment from Negative Ions Using Equation-of-Motion Coupled-Cluster Dyson Orbitals. *J. Chem. Phys.* **2009**, *131*, 124114.